Estimation of blade loads for a variable pitch Vertical Axis Wind Turbine with strain gage measurements

LeBlanc, Bruce; Ferreira, Carlos

DOI
10.1002/we.2713

Publication date
2022

Document Version
Final published version

Published in
Wind Energy

Citation (APA)
LeBlanc, B., & Ferreira, C. (2022). Estimation of blade loads for a variable pitch Vertical Axis Wind Turbine with strain gage measurements. *Wind Energy*, *25*(6), 1030-1045. https://doi.org/10.1002/we.2713

Received: 16 July 2021 | Revised: 6 January 2022 | Accepted: 11 January 2022

DOI: 10.1002/we.2713

RESEARCH ARTICLE

WILEY

Estimation of blade loads for a variable pitch Vertical Axis Wind Turbine with strain gage measurements

Bruce LeBlanc | **Carlos Ferreira**

Wind Energy, Delft University of Technology, Delft, South Holland, Netherlands

Correspondence
Bruce LeBlanc, Wind Energy, Delft University of Technology, Kluyverweg 1, Delft, South Holland 2629HS, Netherlands.
Email: b.p.leblanc@tudelft.nl

Funding information
Wind Op Zee / S4VAWT, Grant/Award Number: TEHE117057; RVO, the Netherlands Enterprise Agency

Abstract

The blade pitch of a Vertical Axis Wind Turbine can have a profound impact on the aerodynamic loading experienced by the turbine. This in turn impacts the structural loads and the performance of the machine. In order to characterize the effects of changing pitch, studies are conducted with fixed pitch offsets from a neutral pitch position in the open jet wind tunnel of TU Delft. Measurements with strain gages bonded to the turbine struts are used to estimate the normal loading of the blades. The measured behavior gives insights into the sensitivity of the turbine loading to the blade pitch angle. Aerodynamic phenomena associated with VAWTs are evident in the data including dynamic stall and blade vortex interaction. Shifting of turbine blade pitch is shown to alter the azimuthally varying normal loading, causing changes in magnitude and direction of rotor thrust. Frequency responses of the turbine and platform mounting structure are presented for rotating and fixed reference frames, respectfully. The effects of stall due to high pitch offsets is shown to excite higher per rev frequencies in both the rotor normal measurements and platform accelerations. The data sets are made available for validation of numerical models.

KEYWORDS
active variable pitch, circulation control, experimental normal loading, VAWT

1 | INTRODUCTION

The blades of a Vertical Axis Wind Turbine experience complex loading every rotation, including swapping pressure and suction sides, unsteady aerodynamics, dynamic stall, blade vortex interaction, and tower shadow. Each of these phenomena can be difficult to simulate, especially at the fidelity of an engineering model, which is generally used in design and lifetime assessment of the turbines. The blade pitch angle of the VAWT has a profound impact on the azimuthally varying loading of the blades. As shown by Ferreira and Scheurich,[1] for a 2D VAWT in potential flow, the power extracted by the turbine can be viewed independently of the azimuthal blade loading by applying fixed pitch offsets which have the effect of shifting the loading between the upwind and downwind passes of the blades. However, in practice, this shifting causes the operation point on the airfoil polar to change corresponding to the pitch angle shifts. With real airfoils, dynamic stall is encountered altering the energy extraction from the flow and leading to complex loading scenarios which are difficult to model.

Few data sources exist in the literature for calibration and validation of numerical models with blade loading at many azimuthal positions. A review of experimental results available for vertical axis wind turbines was published by Battisti et al[2] which highlighted some gaps in the available literature on experimental campaigns. Typically models are calibrated based upon overall rotor integrated loads such as power and thrust

coefficients. For instance, the effects of blade preset pitch on power coefficient versus tip speed ratio were studied by Klimas and Worstell.[3] While useful as a baseline, these comparisons can miss many details of the blade loading which are crucial for the design and development of Vertical Axis Wind Turbines, especially in situations where individual variable blade pitch is considered. As part of the validation campaign for the development of a vortex model for the Darrieus turbine (DART), Strickland and Nguyen[4] published a dataset from a drag tank facility for a straight bladed VAWT at multiple tip speed ratios. Data were also collected in a wind tunnel test by Vittecoq and Laneville[5] showing normal and tangential load data for a VAWT with a chord to radius solidity ratio of 0.2. While data were only collected at a handful of locations around the azimuth, it provides excellent detail of the potential presence of dynamic stall at tip speed ratios lower than 3.5 for said solidity ratio. More recently, measurements have been made using flow analysis techniques such as Particle Image Velocimetry,[6] previously used by Ferreira,[7] Castelein et al,[8] and Castelein.[9] While very useful, these measurements are limited in temporal and azimuthal resolution and are difficult to conduct. Force measurements were made by Uppsala University[10–12] using load cells between the strut connection points and the tower for parked conditions. These measurements were made in both parked and operating conditions for a larger 12 kW machine in the field. The data are very useful as a real-world check. However, due to being field measurements, the wind conditions are not controlled, which adds a level of difficulty for comparison to models for validation. The datasets provided herein look to extend these data sources to include a higher azimuthal resolution in a controlled wind tunnel environment allowing the detailed exploration of the effects of variable blade pitch on the load experienced by the blades.

Experimental data with a high degree of azimuthal resolution is required in order to assess the performance of the simulations at capturing the above-mentioned aerodynamic phenomena. With this in mind, a sensor system was designed for a two-bladed variable pitch H-type vertical axis turbine at TU Delft to discern blade normal loading and azimuth position in multiple blade pitch configurations. Data are presented for seven fixed pitch cases establishing loading trends of the turbine based upon pitch configuration. All data are made available on the 4TU.ResearchData web server.[13]

2 | METHODS

The experiments are carried out using the PitchVAWT wind turbine, developed at TU Delft for studying the effects of variable blade loading on the VAWT and for model validation. For a more detailed look on the design of the machine, see previous works.[14–16] This section provides a brief overview of the turbine, the coordinate systems used, the measurement techniques, and a description of the test campaign.

2.1 | Turbine overview

The experimental turbine, referred to as PitchVAWT, is a two bladed H-shaped Vertical Axis Wind Turbine with individual pitch control. Two horizontal struts support each blade. These are located at approximately 25% and 75% of the blade height to minimize deflection during operation. The blades and struts are manufactured from extruded aluminum, while the tower is made from steel with an outer diameter of 0.06 m. More specifics are given in a previous publication specifically addressing the creation of a calibrated finite element model of the turbine.[15] General turbine specifications are given in Table 1. The as-built diameter of the turbine is 1:48 m and the NACA0021 blade airfoils have a chord length of 0:075 m giving a chord to radius ratio of approximately 0.1. Dimensions and a layout of the turbine are given in Figure 1.

Each blade pitches about the center of mass of the built airfoil at $0.48c$ in order to minimize torque from the centripetal acceleration of the blades on the pitch control motors. The pitch of each blade of the turbine is controlled by an independent motor and can therefore be configured to test most conceivable pitch schemes in the relatively controlled environment of the open jet facility (OJF). The motors for each blade are attached with brackets close to the tower. A steel reinforced belt mounted just below the lower strut is then used to translate the pitch position to the blades using a 1:1 drive gear and sprocket system. More detail can be seen in the previously published design overview paper.[14] Calibration of blade pitch position is performed with a laser alignment system prior to each test. This ensures alignment of zero position for blade pitch and turbine azimuth with reference to the opening of the wind tunnel. Turbine rotational speed is directly controlled using a DC motor controller. This speed is varied in order to achieve a range of tip speed ratios when the wind speed is held constant.

2.2 | Definition of coordinate systems

The coordinate system used for the study is given in Figure 2. The turbine was mounted in the wind tunnel such that the incoming flow comes from the 90° azimuth position, with the x direction following the direction of the wind. The turbine rotates counter-clockwise, and the y direction is defined using the right-hand rule. Forces are defined from the perspective of the force acting on the flow. Therefore, a force acting on the flow in the outward facing normal from the surface of rotation is defined as positive.

TABLE 1 PitchVAWT design specifications

Property	Dimension
NBlades	2
NStruts	4
Rotor height	1.508 m
Diameter	1.48 m
Blade chord	0.075 m
Strut chord	0.060 m
Solidity	0.1
Tower OD	0.060 m
Blade airfoil	NACA0021
Strut airfoil	NACA0018
Blade pitch axis	48% c
Operating λ at $U = 4$ m s^{-1}	1 to 4

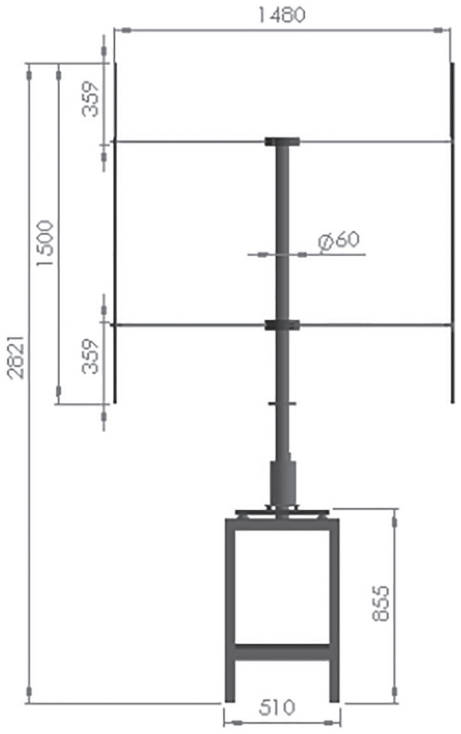

FIGURE 1 PitchVAWT dimensions in mm

The blade pitch, β, sign convention is given in Figure 3. The path of the airfoil is shown with a dashed line. Positive turbine pitch is defined as pitching the leading edge towards the center of rotation, which corresponds to an increase in angle of attack for each azimuth position. Negative blade pitch therefore corresponds to a decrease in α.

2.3 | Wind tunnel facility

Testing of the turbine was conducted in the Open Jet Facility at TU Delft, referred to as OJF. The tunnel is a closed loop open jet test section facility with a 2.85 m $\times$ 2.85 m hexagonal cross-section opening into a 13 m long, 8 m high test section. A schematic showing the layout of the OJF is given in Figure 4. The tunnel is capable of a wind speed range of 3 to 35 m s^{-1}, with a turbulence intensity on the order of 0.5%, evaluated approximately a meter from the outlet of the jet.[17] Due to rotational speed limitations of the wind turbine and a desired tip speed ratio

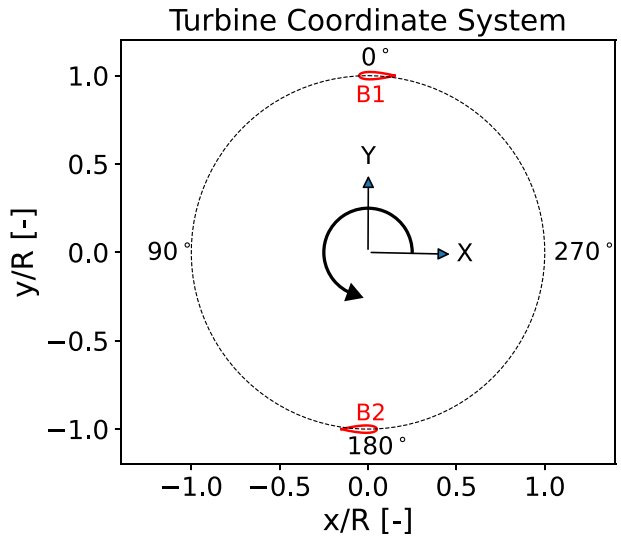

FIGURE 2 Turbine coordinate system, wind approaches from 90°

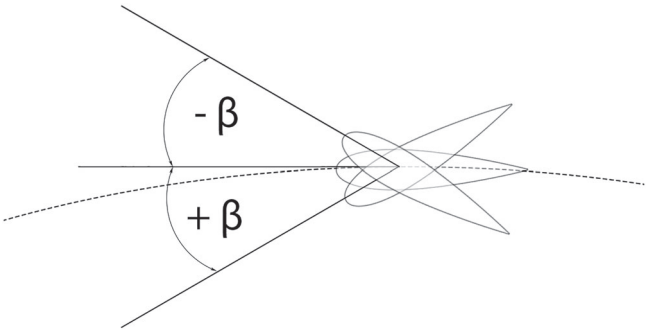

FIGURE 3 Blade pitch convention

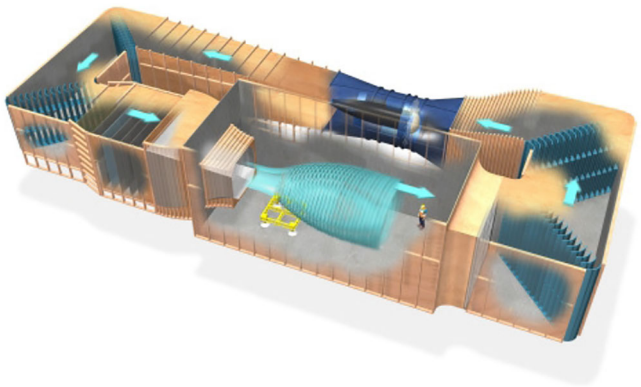

FIGURE 4 Schematic of Open Jet Facility at TU Delft

of operation, wind speeds were limited to 4 m s^{-1} during testing. Tunnel wind velocity is measured with a Pitot tube sensor near the outlet of the jet. A large blue lifting base is available in the tunnel for mounting test hardware. The turbine is mounted to this platform and placed to align in the center of the jet, with the center of the turbine 2 m from the outlet face. A view of the turbine installed in the facility is given in Figure 5. The

tunnel blockage of the turbine as analyzed with respect to AGARDograph 336[18] results in a velocity correction at the mount location within the jet of 0.995. This correction to the data is considered negligible for the analysis performed within this paper.

2.4 | Measurement of rotor speed and azimuth position

The rotor position is measured using a torque transducer with embedded digital incremental optical rotary encoder produced by Burster inc. located between the gearbox and the turbine tower. It is shown installed in Figure 6. The encoder has a 1,600 count = rev or an angular resolution of 0.225°. The encoder is incremental, meaning the zero position needs to be set each time the turbine is powered on. The $\theta = 0^\circ$ position is defined as the angle between the center of the tower and the pitch axis of the machine (.48*c*) being parallel to the tunnel outlet. A laser alignment system is used to set the zero position of the turbine relative to the opening of the wind tunnel outlet. The digital output from the encoder is wired to a DIO module on the PitchVAWT DAQ system. A Field Programmable Gate Array, FPGA, device is then used to convert this signal set to a rotation count and speed. The controller converts the counts from the sensor into azimuth position and the rotation rate of counts per second into revolutions per minute.

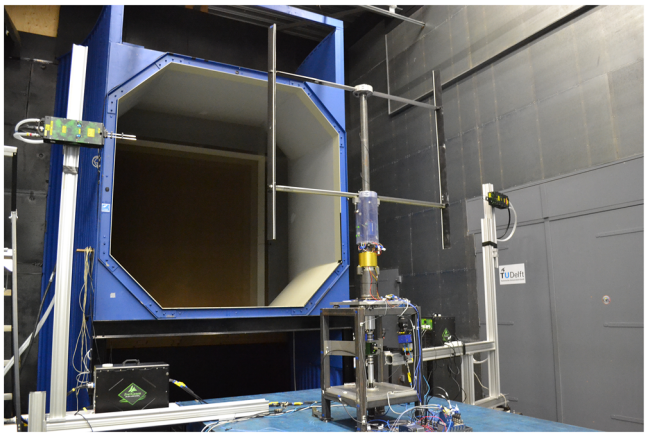

FIGURE 5 PitchVAWT mounted in the Open Jet Facility

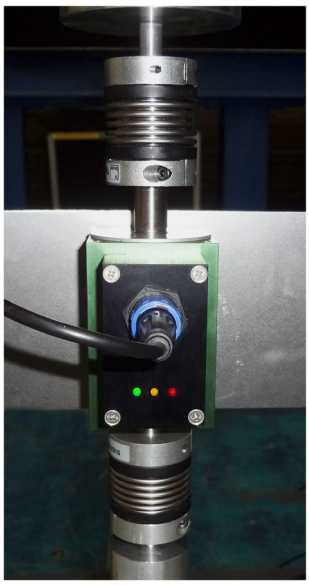

FIGURE 6 Rotary encoder installed on PitchVAWT

2.5 | Measurement of normal load

Blade normal loading is measured utilizing the horizontal extruded aluminum struts used to mount each blade. The struts are a constant cross-section and have the profile of a NACA 0018 symmetrical airfoil. Through work performed creating a calibrated finite element model of the turbine, discussed in a previous publication,[15] the material properties of the struts have been measured experimentally and are given in Table 2. This information is required to transform measured strain to applied normal loading on the strut.

2.5.1 | Measurement and signal conditioning

The normal load is measured using a set of strain gages on the top strut of the first blade of the turbine. A full-bridge strain gage setup is utilized in an axial configuration in order to compensate for any vertical bending or temperature fluctuations which can occur while testing.

In principle, electrical resistance strain gages measure a small change in resistance of a wire due to its elongation ($\epsilon = \delta l / l_0$.) Generally, the strains which occur in materials due to a generic load are very small, on the order of 1×10^{-6}. In order to measure these very small changes, a wheatstone bridge is used; see Figure 7. Each resistor shown in the figure is a strain gage mounted on the structure. Due to each strain gage having approximately the same resistance, when no load is applied to the structure, the bridge is said to be "balanced," and no voltage difference is measured across V_{out}. If the resistance changes on any of the legs due to an applied strain, the circuit will go unbalanced and a voltage will be output to V_{out}. When the gages are applied in a specific way, shown in Figure 8, only the axial strain is measured. This is because any bending load will

TABLE 2 Strut material properties

Property	Dimension
ρ_{strut}	2,620 kg m^{-3}
E_{strut}	55 GPa
$A_{cross-section}$	143 mm^2

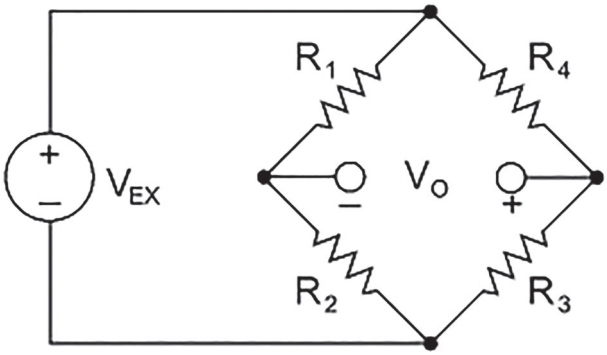

FIGURE 7 Wheatstone Bridge

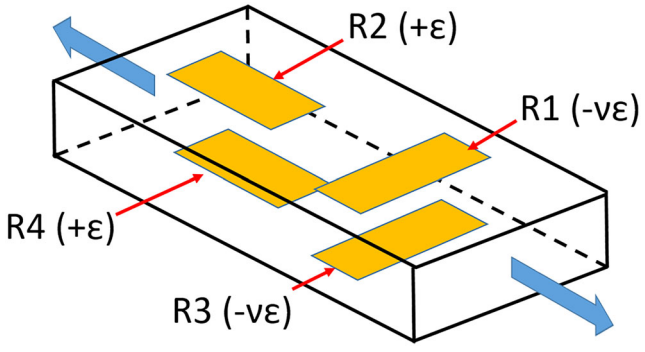

FIGURE 8 Strain gage configuration for axial load

stretch one gage and compress the gage oppositely positioned on the beam the same amount (assuming a symmetrical beam cross-section), therefore keeping the two legs of the wheatstone bridge in balance. This is also true for transverse loading due to Poisson effects and for temperature fluctuations.

The measured voltage out corresponds to the change in resistance of each strain gage as shown in Equation 1.

$$V_{out} = \frac{V_{ex} R_2 R_3}{(R_2 + R_3)^2} \left(\frac{\Delta R_3}{R_3} + \frac{\Delta R_1}{R_1} - \frac{\Delta R_2}{R_2} - \frac{\Delta R_4}{R_4} \right) \tag{1}$$

The voltage due to the strain response is a relative voltage measurement of the measured voltage difference in the wheatstone bridge versus the excitation voltage between strained and un-strained states shown in Equation 2.

$$V_r = \left(\frac{V_{out}}{V_{ex}} \right)_{strained} - \left(\frac{V_{out}}{V_{ex}} \right)_{un-strained} \tag{2}$$

The axial strain can then be attained using the known "strain-gage factor," provided by the manufacturer, the response voltage, and the Poisson's Ratio for the material of the strut (0.33 for aluminum) by using Equation 3.

$$\epsilon_n = \frac{-2V_r}{GF[(\nu + 1) - V_r(\nu - 1)]} \tag{3}$$

Data are collected directly within the PitchVAWT Controller based upon the National Instruments Compact-Rio platform. The strain gage set is wired to an NI 9237 strain gage module. The wires pass through a slip ring up to the top strut for blade 1 of the rotor. A shunt calibration is performed in order to calculate the equivalent voltage drop due to the wiring of the strain gage bridge. However, because a full bridge configuration is used and the gages are placed close together, the local effects of wire resistance are considered negligible. Data are collected within the controller at a rate of 500 Hz. This rate allows capturing the effects of airfoil dynamics directly in the time domain as well as capturing higher frequency content which may be of interest.

2.5.2 | Normal load calculation

First, a calculation is performed to transform the measured strain into a stress. This is performed using Hooke's Law given in Equation 4. The measured strain is multiplied by the known Elastic modulus of the material (given in Table 2). For axial loading, the stress on a cross section is the force on that section divided by the area, Equation 5. For this calculation, the force has only been measured on one of the two struts and is therefore doubled, Equation 6. Due to the symmetrical design of the blades and struts, the assumption that the normal loading is equally distributed among the struts is considered valid.

$$\sigma_n = E\epsilon_n, \tag{4}$$

$$F_{n_{strut}} = \sigma A_{cross-section}, \tag{5}$$

$$F_{n_{blade}} = 2F_{n_{strut}}. \tag{6}$$

A correction is then performed to remove the large load due to the rotation of the turbine around the vertical axis. The mass of the blades and struts is located at a radius removed from the rotational axis. This causes a substantial centrifugal load which corresponds to the suspended mass having an acceleration proportional to the square of the rotational frequency. For a point mass, this can be simplified to $F_{cent} = mr\omega^2$. However, for the turbine, this is a fairly complex phenomenon to perfectly correct for with such an assumption. For the processing, here, a second-order polynomial was fit to the normal load data with respect to the rotational frequency. This accounts for any non-linearities built into the system, as well as the exact sprung mass outboard of the strain gage placement. This correction is given in Figure 9. The polynomial is then used to relate a given measurement point to the load offset based upon the rotational speed. This offset is subtracted from the measurement to give the corrected normal load without the rotational effect.

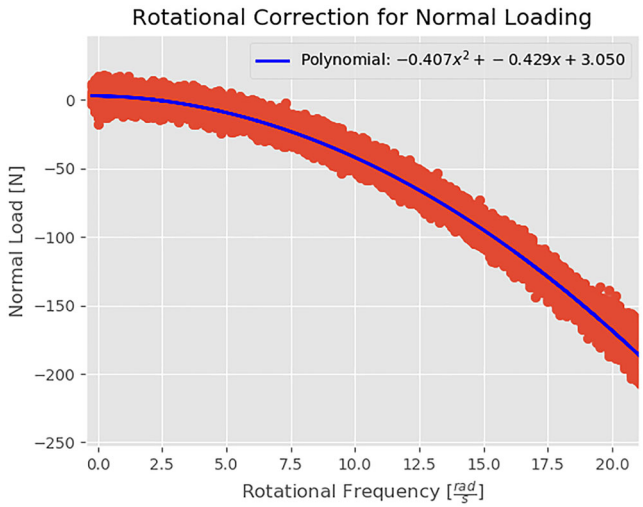

FIGURE 9 Rotation correction for Normal loading

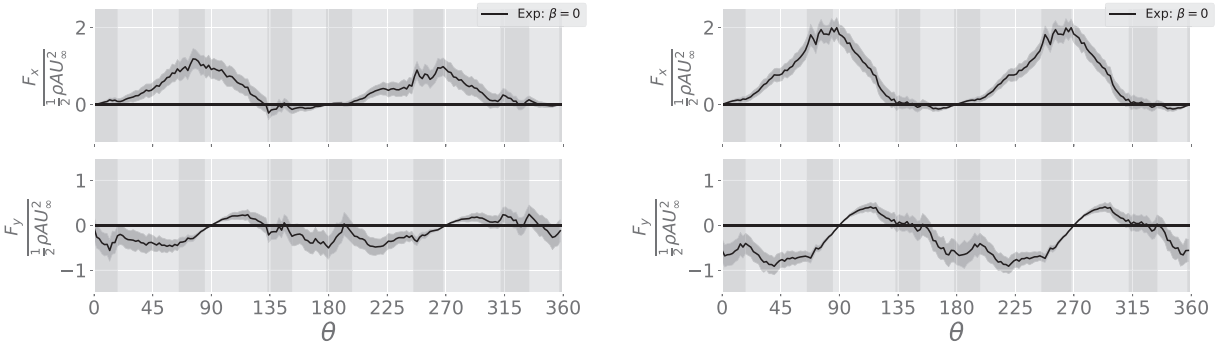

(A) Thrust from Blade 1

(B) Total thrust assuming both blades

FIGURE 10 Thrust from blade normal loads: (A) blade load from single blade; (B) total rotor thrust. Shaded region behind each curve represents $\pm\sigma$ of the binned measurement. Darker vertical shade regions represent areas with additional slip-ring noise

2.6 | Calculation of thrust from normal load

The most direct way to measure the aerodynamic thrust for the PitchVAWT is to convert the blade normal loading as measured above into *x* and *y* components. If each rotor blade had a set of strain gage measurements, this would entail simply summing up the loads over each blade as a function of azimuth position. However, due to channel limitations in the slip-ring of the PitchVAWT, the normal load is only measured for a single rotor blade. As the second rotor blade is designed to mirror the first blade, and the rotor is balanced, the assumption can reasonably be made that it behaves like that of the first. So by sampling the azimuthal load distribution of the first blade with a 180° offset, it is possible to estimate the experienced aerodynamic thrust load for both blades over the rotation of the turbine. The *x* and *y* loads from the measured normal load are given first for the individual blade measurement and then for the assumption of both blades in Figure 10.

2.7 | Normal load assumption

Due to inherent difficulties with directly measuring the tangential loads on each blade, an assumption is made that measuring the normal loading at each azimuth position provides a good representation of the total turbine loading. In order to verify this assumption, a simple study is performed using the 2D Actuator Cylinder Model[19] with an inviscid airfoil polar formulation for the same chord to radius ratio and at the same tip speed ratio as the experiment. The turbine thrust is calculated from the model with and without inclusion of the tangential force vector. Figure 11

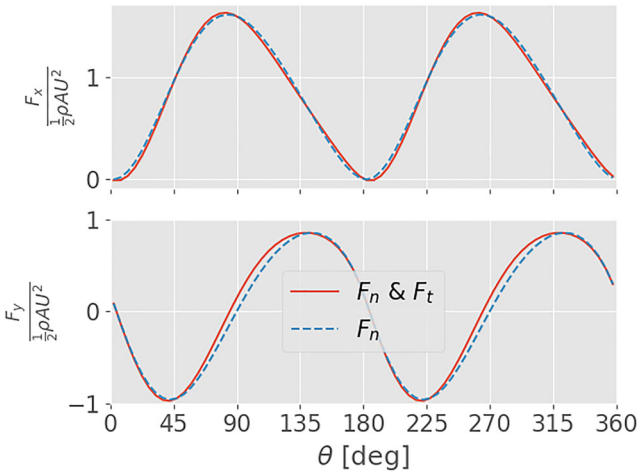

FIGURE 11 Thrust with and without tangential load, from Actuator Cylinder Model

TABLE 3 Integrated thrust values

Pitch	Parameter	Magnitude	Direction
0°	F_n, F_t	.843	89.93°
	F_n	.848	92.58°

and Table 3 highlight the effect of ignoring the tangential component of the blade forces on the calculated thrust magnitude and direction. In the direction of the wind, the difference is negligible; however, there is a slight underestimation of the cross-flow thrust. This underestimation leads to a offset in calculated thrust direction of approximately ±2.5° for the current model. This error is considered acceptable for the current analysis. However, depending on the purpose of the study, this may need to be taken into account.

2.8 | Experimental setup

Testing is conducted with the PitchVAWT turbine in the Open Jet Facility, OJF, of TU Delft. The wind speed was held constant throughout testing at 4 m s^{-1}. The turbine was operated at a constant tip speed ratio of $\lambda = 4$, for an average rotational speed of about 205 RPM. These speeds are chosen due to a resonance which occurs at roughly 215 RPM due to crossing with the backward whirling mode of the tower. At a $\lambda = 4$, most of the deleterious effects of dynamic stall are minimized, allowing the loading changes due to small pitch angle deltas to be measured. Therefore, the wind speed was lowered in order to allow this tip speed ratio at the upper limit of RPM without initiating the resonance with the tower backward whirling mode. For more details, see the previous publication on the dynamic characterization and model development of the PitchVAWT.[15]

The loading over time is binned into azimuthal buckets for understanding the loading over the rotation. The turbine is divided into 180 azimuthal bins of 2°. Each measurement is binned based upon the azimuth position at the time the measurement was taken. The mean and standard deviation are then calculated for each azimuthal bin. Due to the sampling, each measurement bin has a potentially different number of counts. The range of counts per bin was 178 to 216 for testing at the zero pitch, $\beta = 0°$ position, with similar counts for each pitch configuration.

The strain signals are passed through a slip ring in order to transfer the data from the rotating frame of the rotor to the fixed frame of the turbine base. In this process, noise was introduced into the signal at several distinct points along the azimuth position giving a higher uncertainty in these measurements. Data have been collected with no turbine loading in order to quantify the effect of the slip ring in these areas and to remove any localized bias; however, some dynamics exist which are not considered representative of the aerodynamic flow such as sharp inflection points and, therefore, should be treated with care. A vertical shaded region in the plots highlights these sections of the data. As there are ample sections of high-quality data for comparison from test to test and from test to model, there is minimal information lost. Other potential sources of uncertainty include strain gage placement, as it is necessary to align the gages with the axial direction any deviation will cause cosine losses of voltage change; material properties, stiffness, and density were directly measured experimentally several times on a spare turbine strut to minimize any deviation; however, there is a small error associated with all data collection; Poisson's ratio for the strut material is assumed on best practice with aluminum, however has not been directly measured with this turbine. These sources of error are generally much smaller than the overall standard deviation for each measurement bin and are considered to be within the accepted error margin for the measurements.

The mean normal load coefficient ($\frac{F_n}{\frac{1}{2}\rho\lambda^2 U_\infty^2 hc}$) of each azimuthal bin is plotted as a line, with $\pm\sigma$ for each bin given as a shaded region around the line. In order to establish trends in both the positive and negative pitch directions, data are presented for cases where $\beta = 0°, \pm2°, \pm3°, \pm5°$.

3 | RESULTS AND DISCUSSION

3.1 | Azimuthally varying normal load

The baseline loading for neutral pitch with $\beta = 0°$, at the operating tip speed ratio of $\lambda = 4$, is given in Figure 12. The data are presented in two formats: first, in the Cartesian *x*-*y* manner and, then, in polar form to better visualize the effects of the normal loading on the flow of the turbine. Figure 12a displays a graph of the normal force coefficient as a function of azimuth position. The standard deviation of each measurement bin, relayed by the shaded area around the curve, remains consistent over the rotation reflecting a general noise level on the strain measurement. This provides a view of the consistency of the measured load at each azimuth position, as well as the continuity in the turbine loading between each azimuth bin, as no other filters have been applied to the data. The next presentation in Figure 12b shows the same data in a polar format. This plot shows the normal force on the flow around the azimuth position as if viewing the turbine from a top down vantage point, with the wind incoming from the left of the image. The thick black line represents the zero load condition with the red line representing the normal load coefficient at the given azimuth position. Normal load vectors are shown to further enhance the observation of the loading. Total turbine thrust is represented by a large vector stemming from the center of the plot. The normal load is transformed to thrust in *x* and *y* directions using the method discussed in Section 2.6. A trapezoidal integration is then performed over the azimuth for each component of thrust. The components are then used to generate the integrated thrust vector.

Investigating the normal loading for this $\beta = 0°$ condition, the upwind load response between 0° to 90° increases with angle of attack as expected based upon the sinusoidal nature of VAWT aerodynamics of both the apparent wind speed and the expected angle of attack. After the peak loading, as the blade begins to retreat from the wind, between 90° and 180°, the load drops quickly to zero, going negative before the 180° position. This drop is likely due to a reduction in both the angle of attack, and the apparent velocity with the blade retreating from the oncoming wind as well as dynamic stall behavior. The downwind half of the rotor from 180° to 360° shows greater jumps in load than the upwind pass possibly indicating the effect of blade vortex interaction and tower shadow. The resultant thrust vector shows that due to this load reduction in the receding blade after 90°, there is a substantial cross-flow thrust term.

Moving to the variation of loading due to fixed pitch offset cases, the normal loading for each pitch case is provided in polar plot form in Figure 13. The overall trend in the change of load magnitude and direction due to the offset pitch is readily visible. As the pitch increases, the loading shifts earlier in the rotation with the load decreasing post peak at a greater rate, potentially indicating airfoil stalling behavior due to the increasing angle of attack. The opposite occurs for cases with negative pitch offset, with the negative pitch angles reducing the amount of cross-flow thrust experienced by the turbine. Indicating a lower angle of attack delaying the onset of any stall behavior in the upwind portion of the rotation.

The normal load responses for each pitch are directly compared in Figure 14. The neutral pitch of 0° appears to be partially stalled due to the rapid drop off of normal load after the peak. As the blade pitch is increased, this effect is exaggerated, forcing the load higher earlier in the rotation, however also stalling deeper and earlier. With the negative pitch angle, a different response is witnessed. The loading begins the rotation below the neutral pitch case and then continues to increase in loading beyond where the zero pitch case does, perhaps due to less stall on the upwind half. This however also reaches a maximum, and the effect is not seen to increase after $\beta = -3°$ pitch case. The behavior is mirrored in the

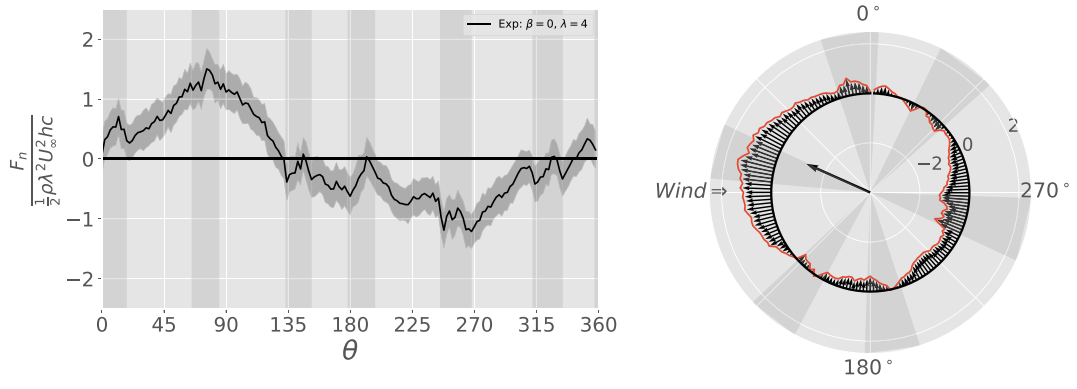

(A) Normal load over azimuth

(B) Polar plot highlight normal load and resultant thrust

FIGURE 12 Normal load coefficient with $\beta = 0°$, $\lambda = 4$

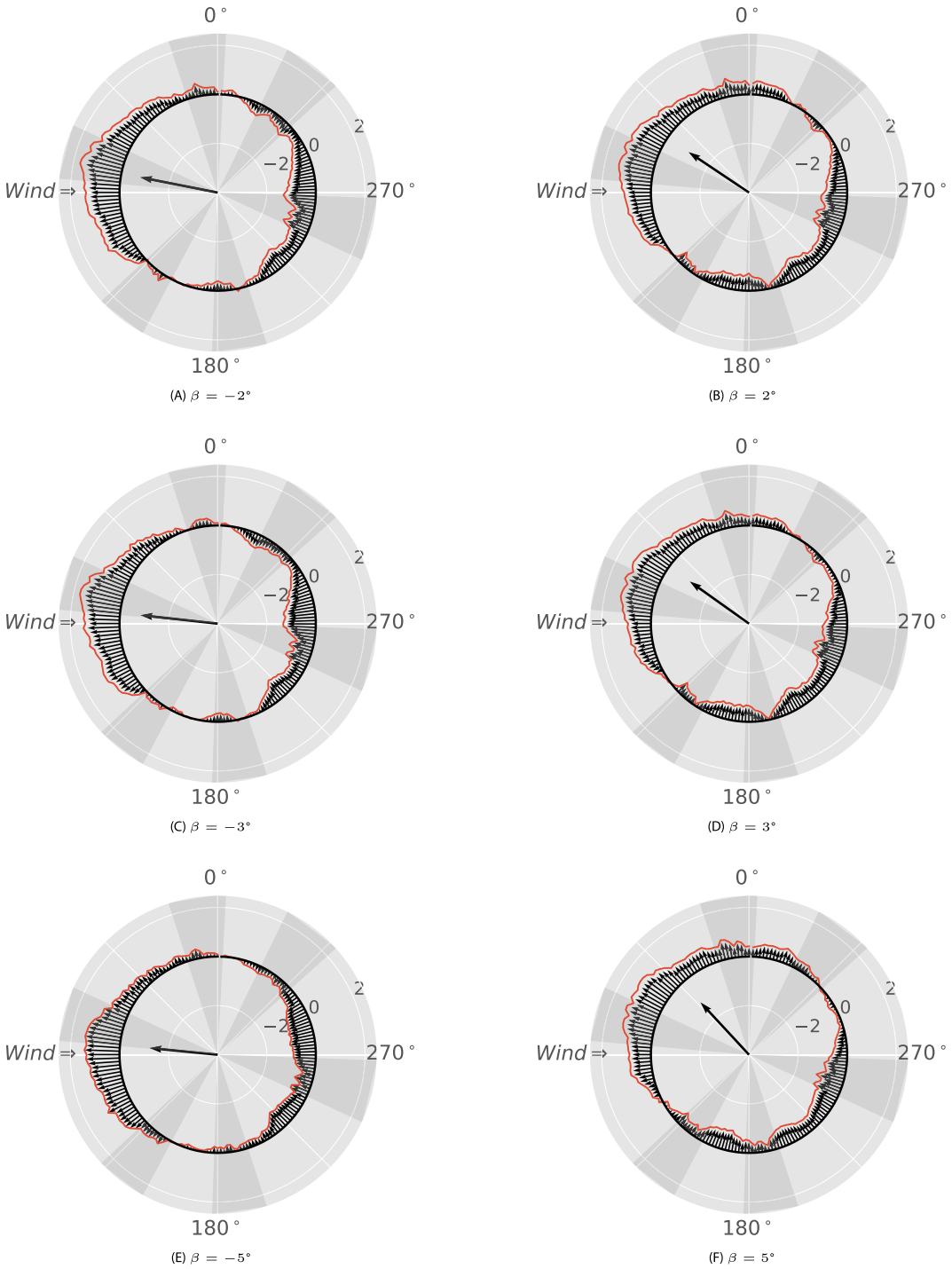

FIGURE 13 Normal load coefficient with fixed pitch offset of PitchVAWT with the integrated thrust vector, $\frac{F_n}{\frac{1}{2}\rho\lambda^2 U_\infty^2 hc}$

downwind half of the rotor, as to be expected with the inversion of the pressure and suction sides of the airfoil on the downwind half. The direct comparison between the extremes of the pitch angles highlight the above analysis more directly.

Thrust coefficients are calculated for each pitch configuration using the normal load distribution as described in Section 2.6. These are given for both the oncoming wind direction, x, and the cross-flow direction, y, in Table 4. The thrust magnitude and direction relate more clearly the above stated relationship with pitch angle. The $\beta = 0°$ case represents the minimum in the magnitude of the thrust vector. Increasing the pitch any further causes a more drastic shift in the direction of the thrust while having a minimal effect on the magnitude; this is likely due to the airfoil already being partially separated in the upwind half of the rotation at the zero pitch condition. With the pitch slightly negative at the $\beta = -2°$ and $-3°$ positions, the magnitude of the thrust is greater and more directly aligned with the flow direction. At a pitch of $-5°$ the thrust magnitude decreases due to a lack of loading on the downwind half of the rotor, most likely due to stall on that half.

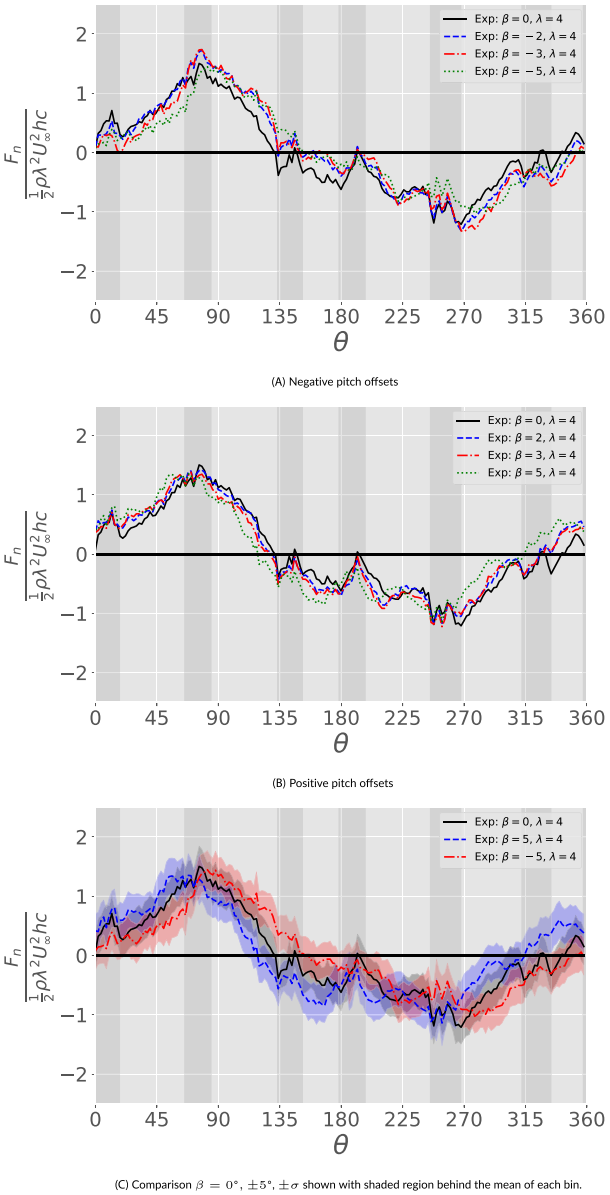

FIGURE 14 Experimental normal load coefficient for negative and positive pitch offsets measured using the PitchVAWT strain gage data

3.2 | Frequency response in fixed and rotating reference frames

The frequency content of the loading provides insight into the data from a different perspective, especially when categorizing important information for fatigue load estimation or dynamic instabilities. This section presents the power spectral density of the normal load measurement for the extremes in turbine pitch compared to the baseline of $\beta = 0°$. The frequency response of the platform is also measured, giving a comparison of the response between the fixed and rotating reference frames.

The power spectral densities of the normal loading for $\beta = -5; 0; 5°$ are plotted against the nondimensional frequency of cycles per revolution in Figure 15. As the normal load is measured in the rotating reference frame, the major response corresponds to the frequency of rotation at 1P. All three pitch cases show the same behavior with the 1P frequency response, as to be expected with the sinusoidal nature of the loading discussed in previous sections. The area of interest occurs in the higher order harmonics, where differing blade loading characteristics such as dynamic stall or blade vortex interaction can take place. With the first three harmonics, the behavior of each pitch condition is consistent with the baseline. However, there is a greater response in the pitched conditions than the zero pitch baseline where greater stall exists in the 3p, 4P, 8P, and 10P frequencies, meaning the stall exacerbates loading at higher per rev frequencies than is seen in the zero pitch case.

A set of single axis PCB 352A24 100 mV/g accelerometers are mounted to the large blue base measuring the platform motion in the *X*, *Y*, and *Z* directions. The accelerometers were mounted on the corner of the platform in order to properly capture the motion for all frequencies of

TABLE 4 Thrust coefficients from normal load data in axial and cross flow directions for fixed pitch cases

β (°)	C_{Tx}	C_{Ty}	Magnitude	Direction (°)
0	.68	−.28	.73	−22.3
2	.63	−.42	.76	−33.5
3	.63	−.45	.78	−35.9
5	.52	−.55	.75	−46.9
−2	.84	−.14	.86	−9.7
−3	.85	−.05	.85	−3.6
−5	.78	−.05	.78	−3.5

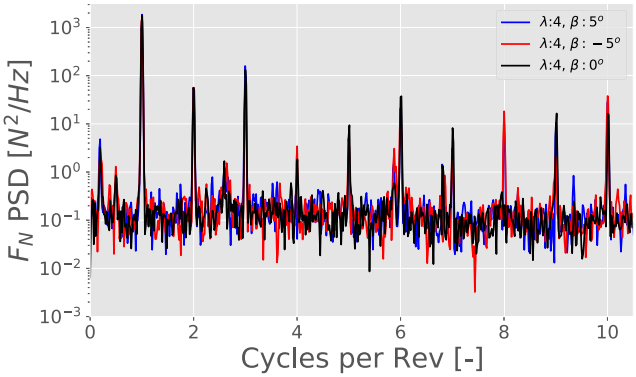

FIGURE 15 Power Spectral Density versus Cycle per Revolution for Normal Force, comparing pitch angles

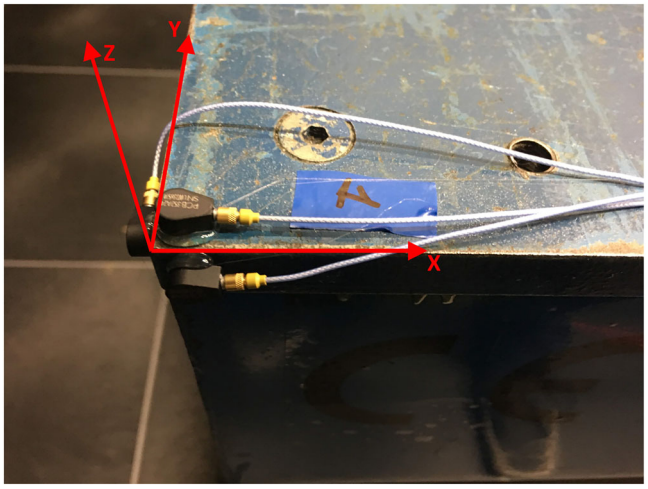

FIGURE 16 Accelerometers mounted to platform with turbine coordinate system

interest by avoiding any node locations. The accelerometers and corresponding directions are shown in Figure 16. As a reminder, the *x* axis is aligned with the incoming flow, the *y* axis is perpendicular to the flow, and the *z* axis is vertical.

The platform motion as measured by the accelerometers is given in Figure 17. The stiffness of the platform is quite different in each direction, with the *X* direction being stiffest followed by the *Y* direction, with the vertical stiffness relatively free in comparison. This is due to the general construction of the scissor lift-based system, and the relative geometry, with the *x* direction aligning with the longest side. This is proven out by the relative responses in each of the directions for all pitch cases. For a more thorough breakdown of the dynamics of the platform, please see the experimental characterization and modeling of the turbine system previously published.[15] The fixed reference frame shows the fundamental excitation frequency for each direction to coincide with the 2P frequency as expected with the two blades of the turbine. The *x* direction response shows both 2P and 4P excitation with very little in response at higher frequencies. There is little difference in response with respect to changing pitch. The *y*-direction response is heavily dominated by the 2P side-side effect. There is more excitation for the 3P and 4P side loads

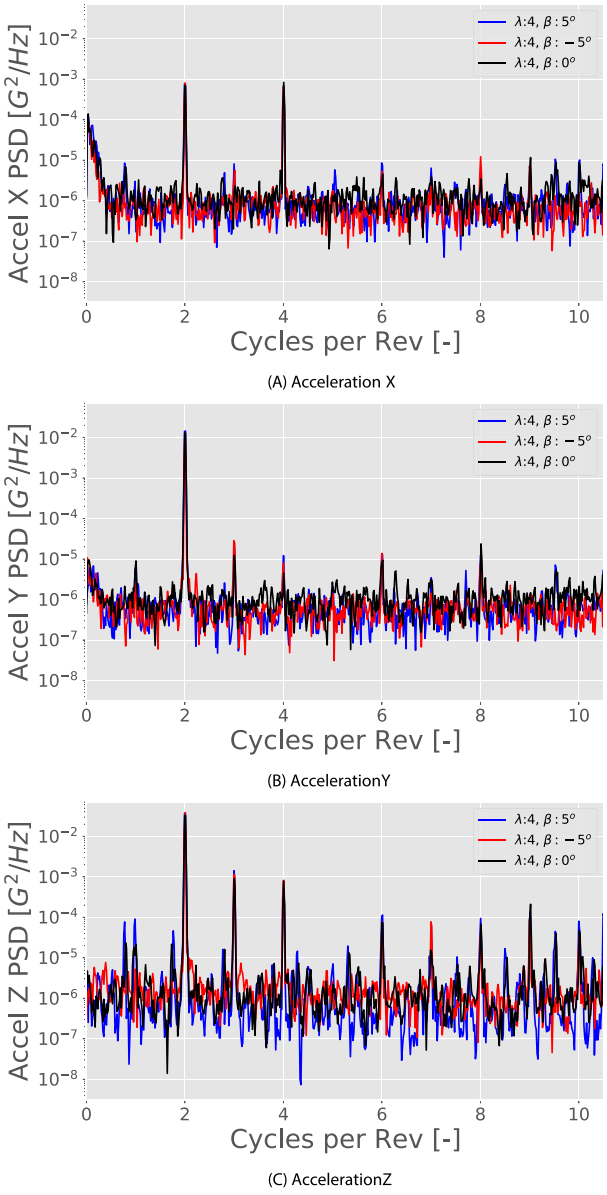

FIGURE 17 Power Spectral Density of platform acceleration

with both the positive and negative pitch offsets. This may be due to the increased side-loading experienced with the offsets due to earlier onset stall. The most excitation in the higher frequencies occurs in the vertical direction. As the platform is effectively "floating on springs" due to the nature of the scissor lift configuration, there is less stiffness in the vertical direction. The moment-arm from the thrust loading causes a rotation about the turbine base which is measured by the acceleration on the corner of the platform. Each pitch case is consistent with response at the 2P, 3P, and 4P peaks, however begin to diverge in the higher frequencies. The loading at 6P, 7P, and 8P is substantially higher with the effect of pitching. This is potentially due to the effects measured in the 3P, 4P, and 8P frequencies measured in the rotating frame from Figure 15. These results show that it may be important to keep in mind the effects of higher per rev frequencies when evaluating structural loading in conditions where dynamic stall can occur.

4 | CONCLUSION

A series of experiments have been conducted in the Open Jet Facility of TU Delft with the PitchVAWT 2-Bladed H-type Vertical Axis Wind Turbine comparing the effects of blade pitch offsets on normal loading at each azimuth position. A technique for measuring the normal loading of the turbine based upon axial strain gage measurements of the turbine struts was presented.

The measured blade loads generally behave in the manner expected for Vertical Axis Wind Turbines with the suction and pressure sides flipping each rotation. The loading in the upwind half for each blade pitch is fairly smooth indicating a clean inflow behavior, while the downwind pass for each blade pitch condition is considerably more turbulent, showing potential behavior of blade vortex interaction and tower shadow. For positive pitch angles, the loading increases with pitch in the first quarter of the turbine rotation. However, this inverts between $\theta = 90^\circ$ and 180° most likely due to increasing effects of stall behavior. The opposite happens with negative pitch angles, as is consistent with the expected stall behavior in the upwind half of the rotation. In the third quarter of the rotation between $\theta = 180^\circ$ and 270°, the trends continue from the upwind half, where stalled behavior continues as the pressure and suction sides reverse. By the 270° position, the flow has recovered for each pitch case, with the positive pitch angles giving a more positive load and the negative pitch angles more negative. This tendency leads to a trend of turbine thrust having a greater cross flow component in positive pitch angles and being more aligned with the flow direction for negative pitch angles.

Measurements presented are for a given wind condition and tip speed ratio to restrict the analysis to varying pitch angles. Operating at lower tip speed ratios would further increase the relative effects of dynamic stall than those already exhibited within the data and would complicate the analysis further. Operation in different wind speed ranges would have an effect on the chord-wise Reynold's numbers, thereby affecting the local airfoil loading and dynamic stall. However, the relative changes experienced due to shifting blade pitch should remain consistent across Reynold's number scales.

The frequency response of both the normal loading and platform motion were studied. The results indicate the effect of changing pitch conditions excites loading in higher cycles per rev. This is potentially due to the much increased stall behavior for the turbine with bigger fixed pitch offsets. These results warrant more study in lower tip speed ratio operating regions where the turbine may have to operate above rated wind speed when loading is also higher. The dataset can be used as a benchmark to validate numerical models of Vertical Axis Wind Turbines experiencing an array of complex flow phenomena.

ACKNOWLEDGEMENTS

The authors would like to acknowledge the support for this work through both the S4VAWT project within the framework of the TKI Wind op Zee program and the Arkom - Tulyp wind project which is sponsored by RVO, the Netherlands Enterprise Agency, under a sustainable energy subsidy.

CONFLICT OF INTEREST

The authors declare no potential conflict of interest.

PEER REVIEW

The peer review history for this article is available at https://publons.com/publon/10.1002/we.2713.

DATA AVAILABILITY STATEMENT

Data referenced in this paper is made publicly available through the 4TU.ResearchData archive

NOMENCLATURE

β	blade pitch ($^\circ$)
λ	tip speed ratio ($-$)
ν	Poisson's ratio ($-$)
ρ_{strut}	density of strut material (kg m^{-3})
σ_n	normal stress (Pa)
θ	azimuthal position ($^\circ$)
A	cross-sectional area (m^2)
DAQ	data acquisition
DIO	digital input/output
E_{strut}	elastic modulus of strut material (GPa)
F_n	normal force (N)
F_t	tangential force (N)
FPGA	Field Programmable Gate Array
U_∞	free stream velocity (m s^{-1})
V_{ex}	excitation voltage (V)
V_{out}	measured voltage (V)
GF	gage factor ($-$)
OJF	Open Jet Facility, Delft University of Technology

ORCID

Bruce LeBlanc https://orcid.org/0000-0002-2711-2825

REFERENCES

1. Simā Ferreira C, Scheurich F. Demonstrating that power and instantaneous loads are decoupled in a vertical-axis wind turbine. *Wind Energy*. 2014; 17(3):385-396. https://doi.org/10.1002/we.1581
2. Battisti L, Persico G, Dossena V, Paradiso B, Raciti Castelli M, Brighenti A, Benini E. Experimental benchmark data for h-shaped and troposkien vawt architectures. *Renew Energy*. 2018;18:50. https://doi.org/10.1016/j.renene.2018.02.098
3. Klimas PC, Worstell MH. Effects of blade preset pitch / offset on curved-blade darrieus vertical axis wind turbine performance. *Report*. SAND81-1762, Albuquerque, New Mexico, Sandia National Laboratories; 1981.
4. Strickland JH, T. WB, Nguyen T. A vortex model of the Darrieus turbine: An analytical and experimental study. Report. SAND79-7058, Lubbock, Texas, Sandia National Laboratories; 1979.
5. Vittecoq P, Laneville A. The aerodynamic forces for a Darrieus rotor with straight blades. *J Wind Eng Ind Aerodyn*. 1983;15:381-388.
6. LeBlanc B, Ferreira C. Estimation of blade loads for a variable pitch vertical axis wind turbine from particle image velocimetry. *Wind Energy*. 2022;25(2):313-332. https://doi.org/10.1002/we.2674
7. Simā Ferreira CJ. The near wake of the VAWT 2D and 3D views of the VAWT aerodynamics. *Thesis*. Delft, The Netherlands; 2009.
8. Castelein D, Ragni D, Tescione G, Simā Ferreira CJ, Guanaa M. Creating a benchmark of vertical axis wind turbines in dynamic stall for validating numerical models. In: 33rd Wind Energy Symposium AIAA SciTech Forum. American Institute for Aeronautics and Astronautics; 2015.
9. Castelein D. Dynamic stall on vertical axis wind turbines, creating a benchmark of VAWTs in dynamic stall for validating numerical models. *Thesis*. Delft, The Netherlands; 2015.
10. Rossander M, Dyachuk E, Apelfröjd S, Trolin K, Goude A, Bernhoff H, Eriksson S. Evaluation of a blade force measurement system for a vertical axis wind turbine using load cells. *Energies*. 2015;8(6):5973-5996.
11. Dyachuk E, Rossander M, Goude A, Bernhoff H. Measurements of the aerodynamic normal forces on a 12-kw straight-bladed vertical axis wind turbine. *Energies*. 2015;8(8):8482-8496.
12. Goude A, Rossander M. Force measurements on a VAWT blade in parked conditions. *Energies*. 2017;10:15.
13. LeBlanc B, Ferreira C. Pitchvawt data. https://data.4tu.nl/collections/_/5287879/0; 2021.
14. LeBlanc BP, Ferreira CS. Overview and design of pitchvawt: Vertical axis wind turbine with active variable pitch for experimental and numerical comparison. In: AIAA SciTech ForumWind Energy Symposium. American Institute of Aeronautics and Astronautics; 2018.
15. LeBlanc B, Ferreira C. Experimental characterization of H-VAWT turbine for development of a digital twin. In: Manwell J, ed. *North american wind energy association / windtech*: IOP Science; 2019.
16. LeBlanc B, Ferreira C. Experimental demonstration of thrust vectoring with a vertical axis wind turbine using normal load measurements. *The science of making torque from wind (torque 2020)*: IOP Publishing; 2020:11.
17. Lignarolo LEM, Ragni D, Krishnaswami C, Chen Q, Simā Ferreira CJ, van Bussel GJW. Experimental analysis of the wake of a horizontal-axis wind-turbine model. *Renew Energy*. 2014;70(C):31-46. https://doi.org/10.1016/j.renene.2014.01
18. Ashill PR, Binion T, Cooper KR, et al. Wind tunnel wall corrections. BP 25, 7 RUE ANCELLE, F-92201 NEUILLY-SUR-SEINE CEDEX. FRANCE: Advisory Group for Aerospace Research and Development; 1998.
19. Madsen HA. The actuator cylinder. *Report*. 530005953978, Aalborg, Institute of Industrial Constructions and Energy Technology Aalborg University Centre; 1982.

How to cite this article: LeBlanc B, Ferreira C. Estimation of blade loads for a variable pitch Vertical Axis Wind Turbine with strain gage measurements. *Wind Energy*. 2022;1-16. doi:10.1002/we.2713